A Self-Adaptive Wavelet-Based Algorithm for Wave Measurement Using Nautical Radar

Jiaqi An, *Student Member, IEEE*, Weimin Huang, *Senior Member, IEEE*, and Eric W. Gill, *Senior Member, IEEE*

***Abstract*—In this paper, a self-adaptive 2-D continuous-wavelet-transform-based algorithm for extracting wave information from X-band nautical radar images is presented. After investigating the 2-D continuous wavelet transform and its application for radar image processing, it is found that the wavelet scaling parameters will affect the results of wave field analysis. The relation of the scaling parameters to the minimum distinguishable wavenumber is developed using a calibration factor. Optimal empirical values of such calibration factors are determined from a series of simulation data tests for variable wave conditions. An iterative algorithm is then proposed that enables the system to automatically select the optimal calibration factor without requiring a reference to other instrumentation. The algorithm is evaluated using dual-polarized radar data collected on the east coast of Canada. Results of the proposed algorithm are analyzed and compared with *in situ* TRIAXYS wave buoy data as well as that obtained from the conventional 3-D fast Fourier transform (FFT)-based method. The impact of signal polarization on the results is explored. The agreement between the buoy and FFT results indicates that the proposed algorithm is practical and effective as an alternative to the classic 3-D FFT-based method for retrieving ocean wave information.**

***Index Terms*—Nautical radar, wave measurement, 2-D continuous wavelet analysis.**

I. Introduction

In THE present context, sea clutter refers to nautical radar signals reflected from the sea surface, and the fact that its properties correlate with those of the ocean wave regime has been recognized since the early days of nautical radar development in the 1960s [1]. The conventional nautical radar provides consecutive images of the ocean surface, which can be used to derive ocean wave and current information. Most of the research conducted in this field relies on the application of a 3-D fast Fourier transform (FFT) to a series of digitized radar image sequences to obtain such information [2]–[6]. The 3-D FFT-based algorithm has been successfully incorporated into the commercialized Wave Monitoring System (WaMoS) product [3]–[5]. In addition, significant wave heights have been derived using the signal-to-noise ratio [7], shadowing information [8], or the principal components of the radar image sequence [9].

The wavelet transform (WT) has been proposed as another feasible technique for ocean remote sensing applications in addition to the FFT-based analyses such as are used in determining ocean features from 1-D wave buoy records and synthetic aperture radar (SAR) images [10]–[12]. The wavelet approach is particularly applicable to and is frequently used for nonstationary and/or inhomogeneous data analysis [13]. Recently, researchers in Taiwan [13]–[18] have applied a 2-D continuous WT (CWT) to process X-band nautical radar data for wave field analysis. Compared with the classic Fourier analysis, which is used to retrieve global ocean wave features assuming spatial homogeneity within the observed area, the CWT method was found to be able to extract local wave information from areas having inhomogeneous wave fields [13]–[15]. However, numerical simulation testing in their research was conducted on a sea surface elevation map instead of simulated radar images. The modulation of radar imaging by such effects as tilt and shadowing was not considered. Most of the research was focused on nonhomogeneous wave field wavelet-based analysis; the selection and criterion of wavelet parameters under different wave conditions were not explored in detail. Furthermore, only image wavenumber spectra were presented and studied [13], [15]. In [19], an algorithm for extracting wave spectra and parameters using the 2-D CWT was presented. In that research, it was also found that the selection of the scaling factor affects the wave retrieval result. Based on extensive simulated radar images, empirical values of the scaling parameter for variable wave conditions are provided. However, to apply an appropriate scaling parameter, the wave condition must be provided by other tools. This information is often not available.

In this paper, a self-adaptive process of selecting appropriate wavelet parameters to derive wave information is proposed. In Section II, the theory of the WT and its application for wave field analysis are reviewed. In Section III, the relationship of the scaling factor and the minimum distinguishable wavenumber is developed using a calibration factor. The iterative method for determining the calibration factor is also designed in this section. Results from both horizontally polarized (H-pol) and vertically polarized (V-pol) field radar data are provided in Section IV. In this section, comparison with the results retrieved from the conventional 3-D FFT method as well as the *in situ* buoy record are also implemented. A conclusion and a brief outline of future work are given in Section V.

Manuscript received June 26, 2013; revised November 15, 2013 and January 17, 2014; accepted May 12, 2014. The work of W. Huang was supported in part by the Research and Development Corporation (RDC) Industrial Research and Innovation Fund under Ignite Grant 207765 and in part by the Natural Sciences and Engineering Research Council of Canada (NSERC) under Grant NSERC 402313-2012. The work of E. Gill was supported in part by the NSERC under Grant NSERC 238263-2010 and in part by the Atlantic Innovation Fund Award. This work was also supported by the RDC Ocean Industries Student Research Award under Grant 208695.

The authors are with the Faculty of Engineering and Applied Science, Memorial University of Newfoundland, St. John's, NL A1B 3X5, Canada (e-mail: jiaqi.an@mun.ca; weimin@mun.ca; ewgill@mun.ca).

Color versions of one or more of the figures in this paper are available online at http://ieeexplore.ieee.org.

Digital Object Identifier 10.1109/TGRS.2014.2325782

II. Two-Dimensional WT and Its Application for Wave Field Analysis

A. Two-Dimensional WT

The 2-D WT decomposes a signal into a series of wavelets that are scaled, shifted, and rotated versions of the so-called mother wavelet [13]–[21]. For an image $s(\vec{\gamma}) = s(x, y)$, where s and $\vec{\gamma} = (x, y)$ represent the intensity of the pixel and its coordinates in the image, respectively, its 2-D WT, i.e., W, may be written as [20]

$$W(\vec{b}, \theta, a) = C_{\Psi}^{-1/2} a^{-1} \int_{R^2} \Psi^* \left(a^{-1} r_{-\theta}(\vec{\gamma} - \vec{b}) \right) s(\vec{\gamma}) d^2\vec{\gamma} \quad (1)$$

where $\vec{b} = (b_x, b_y)$ is a shifting parameter that indicates the shifted position of the wavelet in the space domain; a is a nondimensional scaling parameter that is related to the dilated spatial frequency (wavenumber) of the space domain, whereas a^{-1} normalizes all the dilated wavelets to equalize their energy; Ψ^* is the complex conjugate of the mother wavelet function Ψ; to ensure the invertibility of the WT, the normalization constant, i.e., C_{Ψ}, must satisfy the admissibility condition as found in [13]; θ is a rotation factor, which defines a rotation matrix $r_{-\theta}$ that rotates the wavelet by angle θ in the space domain. This rotation matrix may be written as [13]

$$r_{-\theta} = \begin{pmatrix} \cos\theta & \sin\theta \\ -\sin\theta & \cos\theta \end{pmatrix} \quad (2)$$

where $0 \leq \theta < 2\pi$.

B. Two-Dimensional CWT for Radar Image Processing

The mother wavelet function Ψ in (1) needs to be specified before applying the 2-D CWT to radar images for wave field analysis. Wave measurement requires the specification of a directional mother wavelet. Here, the Morlet wavelet, which can be considered as a bandpass filter with an adjustable passband, is chosen as the mother wavelet [17]. In [13], the Morlet wavelet for the radar image processing was simplified with a peak position at $\vec{k}_0 = (6, 0)$. $\vec{k}_0 = (k_{0_x}, k_{0_y})$ is defined as the peak wavenumber of the mother Morlet function in the nondimensional Fourier space. The Fourier transform of the simplified mother wavelet can be written as

$$\hat{\Psi}(\vec{k}) = e^{-0.5|\vec{k} - \vec{k}_0|^2} \quad (3)$$

which enables $\hat{\Psi}(\vec{k}) = \hat{\Psi}(k_x, k_y)$ to be symmetrical in the x and y directions.

To apply the selected nondimensional continuous Morlet wavelet function to dimensional digital radar image analysis, the 2-D CWT function requires the process of both discretization and sampling. First, the continuous wavelet function in (1) can be discretely rewritten in the form [13]

$$\begin{aligned} &W\left(b_{x_u}, b_{y_v}, \theta_m, a_n\right) \\ &\quad = C_{\Psi}^{-0.5} a_n^{-1} \sum_{p=1}^{N_x} \sum_{q=1}^{N_y} \cdot \Psi^* \left[a_n^{-1} r_{-\theta_m} \left(x_p - b_{x_u}, y_q - b_{y_v} \right) \right] \\ &\qquad \cdot s(x_p, y_q) \Delta x \Delta y \end{aligned} \quad (4)$$

with W being a function of the discrete shifting (b_{x_u}, b_{y_v}), rotation (θ_m), and scaling factors (a_n); (x_p, y_q) are the sample points on the radar image; the subscripts u, v, m, n, p, and q are the discretization indexes; N_x and N_y are the total sampling numbers in the x and y directions of the image; and Δx and Δy are the radar image resolutions in the x and y directions, respectively. Equation (4) is computationally intensive. To reduce the algorithm execution time, it is desirable to perform the CWT in the spatial frequency domain (the Fourier space). This converts the convolutions into multiplications [13] with the result written as

$$\begin{aligned} W\left(b_{x_u}, b_{y_v}, \theta_m, a_n\right) &= C_{\Psi}^{-0.5} a_n \sum_{p=1}^{N_x} \sum_{q=1}^{N_y} e^{i\left(b_{x_u} k'_{x_p} + b_{y_v} k'_{y_q}\right)} \\ &\quad \cdot \hat{\Psi}^* \left[a_n r_{-\theta_m} \left(k'_{x_p}, k'_{y_q} \right) \right] \hat{s} \left(k'_{x_p}, k'_{y_q} \right) \cdot \Delta k'_x \Delta k'_y \end{aligned} \quad (5)$$

where $\hat{s}$ is the FT of the image intensity s. As previously mentioned, $\vec{k} = (k_x, k_y)$ is the wavenumber in nondimensional space and after the WT, $\vec{k'} = (k'_x, k'_y)$ is the wavenumber in dimensional space, where $k'_x \in [-(N_x/2)\Delta k'_x, (N_x/2)\Delta k'_x]$ and $k'_y \in [-(N_y/2)\Delta k'_y, (N_y/2)\Delta k'_y]$, with (k'_{x_p}, k'_{y_q}) indicating the sampled components of $\vec{k'}$. $\Delta k'_x$ and $\Delta k'_y$ are the wavenumber resolutions in the dimensional spatial frequency domain, written as

$$\Delta k'_x = \frac{2\pi}{N_x \Delta x} \quad (6)$$

$$\Delta k'_y = \frac{2\pi}{N_x \Delta y}. \quad (7)$$

After dilation and rotation with parameters a_n and $r_{-\theta_m}$, respectively, the corresponding peak wavenumber in the dimensional space becomes $\vec{k'}$, which satisfies

$$\vec{k}_0 = a_n r_{-\theta_m}(\vec{k'}). \quad (8)$$

Therefore, the 2-D CWT, i.e., $W(b_x, b_y, \theta, a)$, can be written as a function of the shifting factor $\vec{b} = (b_x, b_y)$ and transformed wavenumber $\vec{k'}$. Once the shifting factor is specified as $\vec{b}_0$, a 2-D wavenumber image spectrum $W(\vec{k'})$ at point $\vec{b}_0$ is determined as

$$W(b_x, b_y, \theta, a) \rightarrow W(\vec{b}, \vec{k'}) \xrightarrow{\vec{b}_0} W(\vec{k'}). \quad (9)$$

The derived image spectrum $W(\vec{k'})$ is dimensional. Thus, $\hat{\Psi}^*$ in (5) needs to be sampled, and this process converts the nondimensional wavelet into a dimensional one. As discussed earlier in this section, the matrix $r_{-\theta_m}$ is applied to control the direction of the wavelet function, and k_{0_y} is set to zero so that k_{0_x} controls the peak spatial frequency in the spatial frequency domain [13]. The sampling process and the determination of the corresponding wavelet factors may be simply conducted on the k_x-axis, where the rotation angle $\theta = 0$. In the space domain, if the sampling resolution is Δx m and the total number of sample points is N_s, the total length to be transformed by the mother wavelet used for image analysis in dimensional space is simply

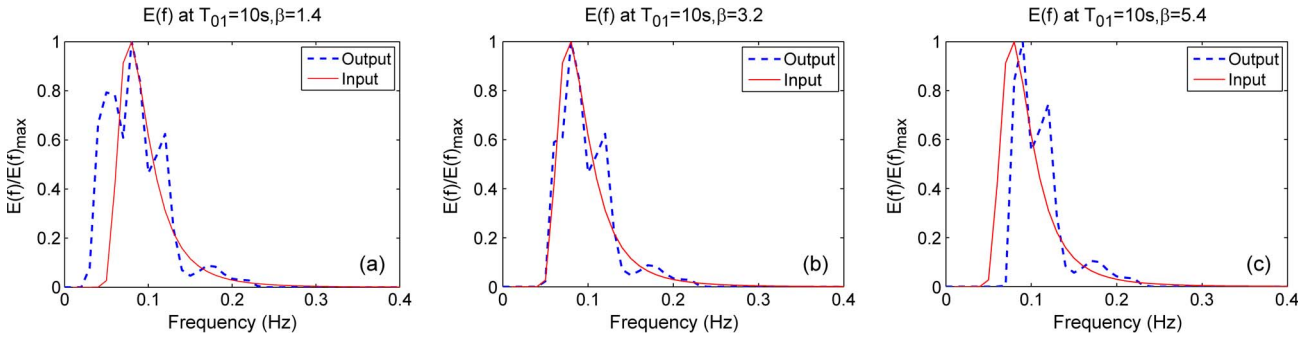

Fig. 1. Example of CWT-derived 1-D spectra $E(f)$ using different β at $T_{01} = 10$ s, $\Delta x = 10.5$ m, and $N_x = 128$. (a) $\beta = 1.4$. (b) $\beta = 3.2$. (c) $\beta = 5.4$.

$X' = N_s \Delta x$ m. If the total length of the mother wavelet in nondimensional space is $X = 2D$, this nondimensional mother wavelet is mapped into N_s points during the sampling process. This may be formally represented as [15], [21]

$$[-D, D] \leftrightarrow [0, N_s \Delta x]. \tag{10}$$

The nondimensional length of the mother wavelet can be determined as $2D = 2 \times 3.5\,\sigma_x$, where σ_x is the standard deviation given in [21]. The minimum number of sample points can be calculated in terms of the Morlet wavelet's nondimensional length as [21]

$$N_s = \frac{2D}{\pi}\left(k_{0_x} + \sqrt{-2\ln(\eta)}\right) \tag{11}$$

where η is a parameter defined in [21] as the ratio of the wavelet value at the cutoff wavenumber k_{c_x} and that at the peak wavenumber k_{0_x}. The value of η is commonly set to 0.01 by Wu *et al.* in [13] and Chuang *et al.* in [15].

III. Scaling Factor Selection and Self-Adaptive 2-D CWT Wave Analysis Algorithm

A. Discussion of Scaling Factors

To obtain the wave field spectrum from the wavelet analysis as indicated in (5) and (9), the scaling factor a_n needs to be specified. In [19], it is simply assumed that a_n takes the form of a geometric progression and is related to the range of the desired spectrum. Here, the selection of the scaling factor for wavelet analysis will be explored in more detail.

First, the relationship of the scaling factor and the desired wavenumber is deduced. It is known that the spatial frequency is inversely proportional to the total length. With $\theta = 0$, it can be shown from (8) and (10) that

$$\frac{k_{0_x}}{\left[a_n\left(k'_x \cos 0 + k'_y \sin 0\right)\right]} = \frac{1/X}{1/X'} = \frac{N_s \Delta x}{2D}. \tag{12}$$

Therefore, the expression of the sampled wavenumber in dimensional space is written as

$$k'_x = \frac{2D k_{0_x}}{a_n N_s \Delta x}. \tag{13}$$

Given the sampled wavenumber range of the image spectrum on the k_x-axis, the maximum value of the scaling factor can be determined by considering (13) with k'_x set to a minimum value given as

$$k_{x'_{\min}} = \beta \Delta\, k'_x \tag{14}$$

and with $k_{0_x} = 6$. Clearly, the maximum value of a_n may then be written as

$$a_{\max} = \frac{2D \cdot 6}{N_s \Delta x \beta \Delta\, k'_x} \tag{15}$$

where β is a calibration parameter that regulates the value of $a_{\max}$. Therefore, we conclude that after the sampling process, the minimum distinguishable value of the wavenumber $k'_{x_{\min}}$ of the dimensional spectrum can be specified by an appropriate selection of the maximum scaling factor or, more specifically, by the selection of the calibration factor β that refines the values of $a_{\max}$.

It is known that with a decreasing mean wave period T_{01}, the peak frequency (wavenumber) increases, and the whole spectrum shifts to larger (spatial) frequency components. Thus, the corresponding minimum distinguishable frequency and wavenumber keep increasing. Therefore, it is reasonable to assume that if Δx and N_x are fixed, for a sea state with smaller mean wave period T_{01}, a larger calibration factor β should be used, as indicated by (14).

Failure to select an appropriate β may result in a less accurate or completely incorrect derivation of wave spectra and parameters. Fig. 1 shows examples of 1-D frequency spectra $E(f)$ derived using the 2-D CWT and using different β for simulated radar images with $T_{01} = 10$ s, $\Delta x = 10.5$ m, and $N_x = 128$. It is observed in Fig. 1 that the derived spectrum using $\beta = 3.2$ agrees best with the input $E(f)$. If a smaller β of 1.4 is used, a fake peak is observed on the left of the spectral peak. If a larger β of 5.4 is used, the derived spectrum is shifted to the right compared with the input $E(f)$. Clearly, the T_{01} values derived from the spectra in Fig. 1(a) and (c) are less accurate. As indicated in Section II-B, the 2-D CWT analysis in the frequency domain is essentially the sum of a series of bandpass filtered signals. The image function $\hat{s}$ is processed with the modified bandpass filters, which are defined by the transformed wavelet functions. The scaling factors control the bandwidths and peak positions of the wavelet series. In [21], it is observed that the larger the

TABLE I
β FOR DIFFERENT T_{01} WITH $\Delta x = 10.5$ m, $N_x = 128$

T_{01} (s)	β
16	1.4-1.6
14	1.7-2.0
13	2.1-2.2
12	2.3-2.4
11	2.5-2.9
10	3.0-3.4
9	3.5-3.9
8.5	4.0-4.5
8	4.5-5.2
7.5	5.2-5.7
7	5.8-6.5
6.5	6.6-7.3
6	7.4-8.4

scaling factor, the closer the peak position will be to the origin. Therefore, an underestimated β in (15) regulates an overestimated $a_{\max}$, which defines undesired filters centered close to the origin. This results in a redundant energy component (a fake peak). On the contrary, an overestimated β will cause missing energy (right-shifted) in the derived spectrum.

As in [19], based on a series of data tests, the empirical values of β for sea conditions with varying T_{01} are shown in Table I. This lookup table is generated under the assumption of deep water and can be applied to both wind sea and swell with a wave period of 6–16 s. Here, only the wave fields with typically observed T_{01} are provided since no satisfactory calibration factors can be found for wave fields from the data test with $T_{01} < 6$ s or $T_{01} > 16$ s. Moreover, the values of β provided in Table I are obtained at a specific image resolution $\Delta x = 10.5$ m and subimage length $N_x = 128$. According to (14), β_n for different Δx_n and N_{x_n} values should be modified as

$$\beta_n = \beta \frac{N_{x_n} \Delta x_n}{N_x \Delta x}. \tag{16}$$

Therefore, once the radar image resolution and the size of the subimage are provided, an appropriate value of β for the 2-D CWT analysis can be determined from Table I and (16), according to the mean period of the wave field to be examined.

Knowing $a_{\max}$ (or β) is not enough to determine all the scaling factors. As previously discussed, the Morlet wavelet in the spatial frequency domain can be regarded as a bandpass filter whose width decreases as the scaling factor increases. It is therefore assumed that a_n takes the form of the geometric progression [21]

$$a_n = M^{n-1}, \quad n = 1, 2, \ldots, N_a \qquad M > 1 \tag{17}$$

where $n = 1$ corresponds to the wavelet without dilation (mother wavelet). Thus

$$a_{\min} = a_1 = 1. \tag{18}$$

The base M in (17) is given as [21]

$$M = \frac{k_{p_1}}{k_d + k_{p_1}} \tag{19}$$

where k_{p_1} indicates the peak location of the 1-D wavelet without dilation as in (18) so that

$$k_{p_1} = k_{0_x} = 6 \tag{20}$$

and k_d is a proportionality constant that is derived from the scale resolution χ as [21]

$$k_d = -\sqrt{-2\ln(\chi)}. \tag{21}$$

The scale resolution $\chi \in (0.0, 1.0)$ is defined in [21] as the ratio of the peak energy of a wavelet with a given scaling factor (a_{n_τ}) to that with the previous scaling factor $(a_{n_{\tau-1}})$. χ near 1.0 or 0.0 represents a high- or low-resolution wavelet series, respectively. For ocean wave analysis, it is determined from simulated and field data tests that an appropriate range of this parameter is given by $\chi \in [0.9, 0.95]$.

B. Self-Adaptive 2-D CWT-Based Wave Analysis Algorithm

After the 2-D CWT analysis, the image spectrum of a radar image is derived. Then, the wave spectrum can be obtained by applying a modulation transfer function (MTF) to the derived image spectrum [3]. In this process, techniques similar to those used in the classic 3-D FFT-based algorithm are employed [22]–[24]. As stipulated in Section III-A, the calibration factor β required for the 2-D CWT cannot be selected until Δx, N_x, and T_{01} are specified. Normally, the information of image resolution Δx and subimage size N_x are available from the system specifications, whereas the value of T_{01} must be obtained from other instrumentation such as a wave buoy. In [19], a lookup table based on the 2-D CWT algorithm is proposed, which requires knowledge of T_{01}. Here, however, an iterative algorithm, which enables the system to automatically select an optimal β without the *in situ* buoy reference, is proposed.

The proposed algorithm is designed to search for an appropriate calibration factor β via the following process.

1) Subimage acquisition and normalization.
2) Generation of an image spectrum by applying 2-D CWT on a single frame of the normalized subimage using an initial β_0. β_0 is set as 1.4 for an image resolution of 10.5 m and a subimage length of 128 pixels. For other resolutions and lengths, β_0 should be modified using (16).
3) Derivation of a 1-D frequency spectrum $E(f)$ and calculation of the mean period, i.e., T_{01}, and application of an empirical threshold to $E(f)$ to check whether any peak (i.e., a point for which the slopes at the two adjacent points have opposite signs) other than the major peak lies above the threshold to the left of the major peak in the derived $E(f)$: If such a point is detected, it is identified as a false peak.
   a) If a false peak is detected, go back to step (2), increase the value of β by $\Delta\beta$ and repeat steps (2) and (3). $\Delta\beta$ should be set small enough so that high-resolution retrieval results can be obtained. However, the computation cost may be high if $\Delta\beta$ is too small. For the image parameters associated with Table I, $\Delta\beta = 0.2$

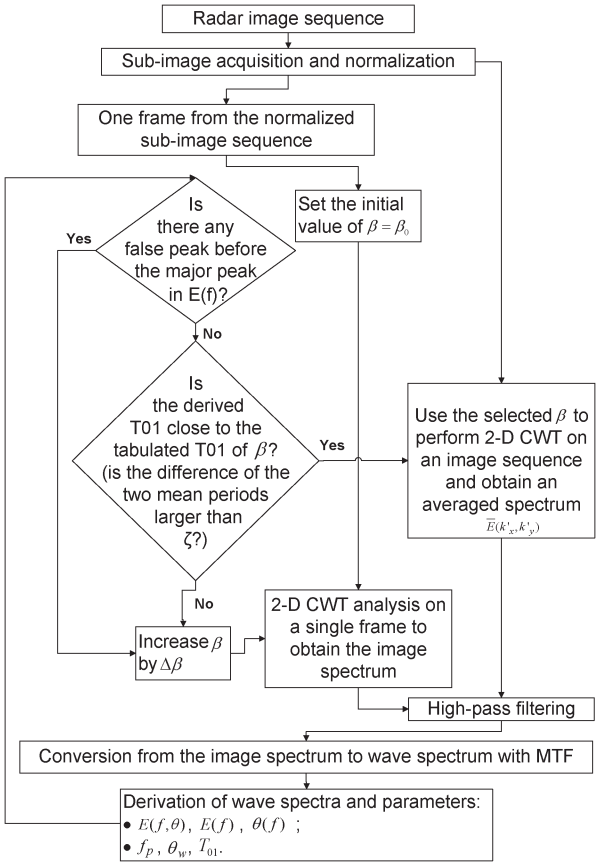

Fig. 2. Flowchart of the self-adaptive 2-D CWT-based wave analysis algorithm.

is set to 0.2. The value should be modified using (16) for other image parameters.

b) If no false peak is detected, compare the calculated T_{01} with the mean period that corresponds to β using Table I and (16).
   i) If the difference of the two mean periods is larger than a preset threshold ζ, increase the value of β by $\Delta\beta$ and repeat steps (2) and (3).
   ii) If the difference is smaller than the specified threshold ζ, β is identified as an appropriate value for wave field analysis. This value may then be used to process the 2-D CWT on the whole radar image sequence, and the derived 2-D directional-frequency spectra $E(f,\theta)$ may be averaged for wave information extraction. In this research, if $T_{01} < 10$ s, $\zeta = 0.5$; otherwise, $\zeta = 1$.

The complete self-adaptive wavelet-based algorithm for the extraction of ocean wave information is depicted in Fig. 2. The sensitivity of the calibration factor to the number of frames has been tested using multiple data sets. It was found that a single high-pass filtered subimage from the normalized image sequence is enough to obtain an approximate calibration factor. Although the T_01 value derived from a single subimage using this calibration factor may contain some error, accuracy can be improved by applying it to a sequence of subimages with averaging. The sensitivity is seen to increase as the wave data become more inhomogeneous.

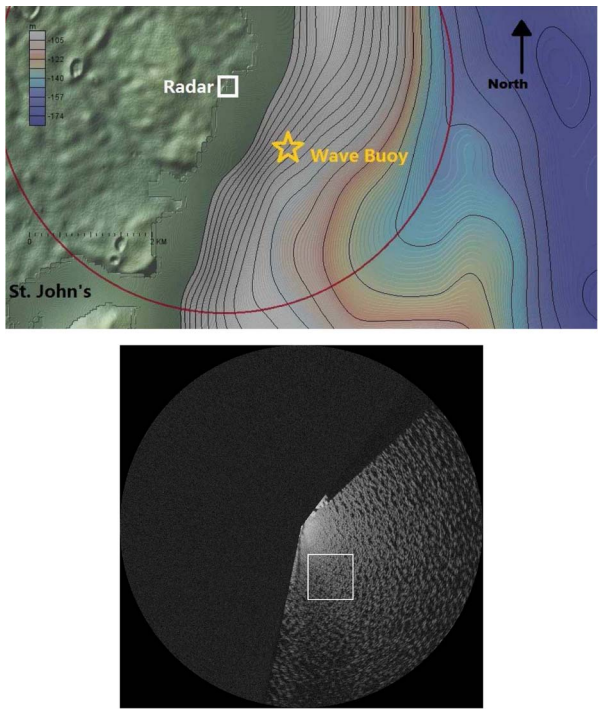

Fig. 3. (Top) Radar and buoy sites. (Bottom) Example of a V-pol X-band nautical radar plan position indicator image on December 15, 2010 and the subimage selection for wavelet analysis. The image and map are oriented in the same manner.

IV. Results and Analysis of Field Data Test

To verify the proposed algorithm, both simulated and field data tests are conducted. In [19], the results of the simulated data test assuming shadowing (SH) and tilt modulation (TM) have been demonstrated. In this paper, two sets of dual-polarized radar field data collected on December 15–20, 2010 at Skerries Bight near St. John's Harbor on the east coast of Canada are first used for the 2-D CWT wave analysis. Data from a TRIAXYS wave buoy record collected at the same time were used as the ground truth [22]–[24]. The sampling period of the buoy is 0.1736 s. The radar and buoy sites are shown in Fig. 3(top). In this figure, bathymetric information is depicted, and the area covered by the radar is enclosed by the red circle. The antenna height is 25.6 m above sea surface, and the distance from the radar antenna to the wave buoy is 1.11 km (0.6 nautical miles). A typical V-pol X-band nautical radar image collected on December 15 is provided in Fig. 3(bottom). The white box of dimensions 128 × 128 pixels shown in the figure depicts the subimages used for wave retrieval. Its center is where the wave buoy was moored. Detailed information on the land-based radar and buoy is given in Table II. Based on the information provided, the parameters assigned for the wavelet analysis are determined and listed in Table III. An initial value of $\beta_0 = 1.6$ and $\Delta\beta = 0.4$ are used for $\Delta x = 10.5$ m and $N_x = 128$. As listed in Table II, the image resolution of the radar field data is $\Delta x = 7.51$ m. Therefore, the corresponding starting β_0 and $\Delta\beta$ values used in this field data test can be calculated as 1.14 and 0.286, respectively, according to (16). For the field data of this section, it was found that the optimal choices of β follow those for the simulations. As discussed in Section III, the threshold ζ

TABLE II
LAND-BASED RADAR AND BUOY DATA INFORMATION

Radar System Specification	
Collecting date	12/15/2010; 12/20/2010
Starting time	16:30:02 (GMT); 13:30:57 (GMT)
Radar location	47.5934N 52.6634W
Polarization	Dual Polarization
Antenna angular speed	48 r.p.m.
Antenna height	25.6 m
Antenna length	2.535 m
Radar pulse length	50 ns
The radar range resolution	7.51 m/pixel
Generated image size	1024×1024 pixels
Buoy Information	
Collecting date	12/15/2010; 12/20/2010
Starting time	16:30:00 (GMT); 13:30:00 (GMT)
Buoy location	47.3362N 52.4210W
Significant wave height	2.20 m; 4.38 m
Wind speed	0.9 knots; 7.3 knots

TABLE III
WAVELET PARAMETER CONFIGURATION

$\vec{k}_0$	$(6, 0)$
χ	0.9
η	0.01
$\vec{b}_0$	$(1, 1)$
N_x	128
Starting β_0	1.001
$\Delta\beta$	0.143

TABLE IV
COMPARISON OF DERIVED PARAMETERS FROM LAND-BASED DUAL-POLARIZED RADAR DATA AND BUOY RECORDS

Wave parameters	$\bar{\theta}$ (°)	T_{01} (s)	f_p (Hz)	H_s (m)
Date	Dec. 15, 2010			
3-D FFT (H-pol)	63.25	7.42	0.105	1.86
2-D CWT (H-pol)	61.39	7.78	0.110	1.65
3-D FFT (V-pol)	63.72	7.93	0.105	1.94
2-D CWT (V-pol)	73.30	7.74	0.105	1.73
Buoy Record	60.47	6.39	0.103	2.20
Date	Dec. 20, 2010			
3-D FFT (H-pol)	38.11	10.76	0.085	4.09
2-D CWT (H-pol)	61.62	10.45	0.080	3.77
3-D FFT (V-pol)	39.23	11.0	0.080	3.92
2-D CWT (V-pol)	62.56	10.42	0.079	3.21
Buoy Record	53.63	9.42	0.075	4.38

used in the iterative algorithm for determining the appropriate calibration factor is 0.5 or 1 depending on whether T_{01} is less than 10 s. The parameter used in the MTF process for the Fourier analysis is determined using the curve fitting technique in [3] and may be written as

$$\mu = \begin{cases} -0.96, & \text{if } |k_{xy}| \le e^{-2.2} \\ -1.2, & \text{otherwise.} \end{cases} \tag{22}$$

Similarly, a modified MTF for the field data wavelet analysis is given as

$$\mu = \begin{cases} -1.42, & \text{if } |k_{xy}| \le e^{-2.75} \\ -1.2, & \text{otherwise.} \end{cases} \tag{23}$$

The retrieved wave parameters are also compared with those from the conventional 3-D FFT-based method.

In the FFT analysis, a sequence of 32 radar images (40-s data) is used as one group to obtain one set of wave parameters. In the 2-D CWT analysis, a minimum number of eight frames are required for satisfactory CWT analysis (see [19]). We found that the results do not change much if more than eight frames are applied in the wavelet analysis; if fewer frames are used, the accuracy significantly decreases. During the field data test, a 20-min radar time series was used for both the 2-D CWT and 3-D FFT analysis (30 groups of 40-s data), and the results were averaged to acquire the directional-frequency spectrum $\bar{E}(f, \theta)$ in each case. For both methods, wave parameters calculated from these two averages are listed in Table IV, in which the *in situ* wave buoy results are obtained by averaging every half an hour. It is obvious that wave direction $\bar{\theta}$ and peak frequency f_p retrieved using both methods are close to the buoy record. The mean periods T_{01} derived from the radar data using both algorithms are slightly larger than the *in situ* buoy recorded value. The significant wave heights H_s, which are calculated as four times the square root of the integral of the retrieved 1-D spectra for the radar data, also agree with the buoy results.

It is worth mentioning that the surface current velocity is not obtained from the proposed 2-D CWT-based algorithm. Thus, the bandpass filtering process that is designed to eliminate the energy offset due to surface current in the 3-D Fourier analysis is not applicable here. In this data set, the wavelet analysis provides similar results as the Fourier method because the currents, as discussed in [23], are relatively small ($u \approx 0.35$ m/s on December 15 and $u \approx 0.47$ m/s on December 20).

Figs. 4–7 show the spectra derived from both the 2-D CWT and 3-D FFT algorithms using the dual-polarized radar data collected on December 15 and 20, 2010. The wave buoy information recorded at the same time is also sketched in the figures. The frequency resolution of both the radar-deduced and buoy-derived spectra is 0.005 Hz. The 2-D directional-frequency spectra [see Figs. 4(a)–(c)–7(a)–(c)] derived by both methods show that the energy distribution is, in general, correctly recovered. The peak frequencies of the radar-derived spectra using both methods are also within 0.01 Hz of those obtained from the buoy reference. Moreover, it is demonstrated by comparing the mean wave direction spectra $\theta(f)_{\mathrm{FFT}}$ and $\theta(f)_{\mathrm{CWT}}$ [see Figs. 4(d)–7(d)] that the wave directions retrieved from the proposed algorithm agree well with those from the buoy record.

It is clear that a second peak near 0.18 Hz appears on the December 15 buoy record of the 1-D frequency spectra [see Figs. 4(e)–7(e)]. The energy of this second peak is detected by the 3-D FFT-based algorithm. However, this second peak is not shown in the recovered curve from the 2-D CWT-based algorithm. This may be because the selected MTF function as described in (23) oversuppresses the energy near the frequency components of $2f_p$. In addition, it is observed in Figs. 4 and 5(e) that both methods fail to recover the energy at very large frequency components ($f > 0.28$ Hz), which results in the overestimated mean period T_{01}. Moreover, in this work, the wave results extracted from V-pol and H-pol data do not significantly differ. Of course, the *in situ* buoy data represent the measurement at a fixed point where the buoy is moored, whereas the radar measurement represents the result from a rectangular area. This may explain why the radar spectra are smoother than those obtained from the buoy.

To further verify the self adaption and robustness of the proposed algorithm, another two sets of ship-borne field data collected on November 28–29, 2008 offshore Nova Scotia are

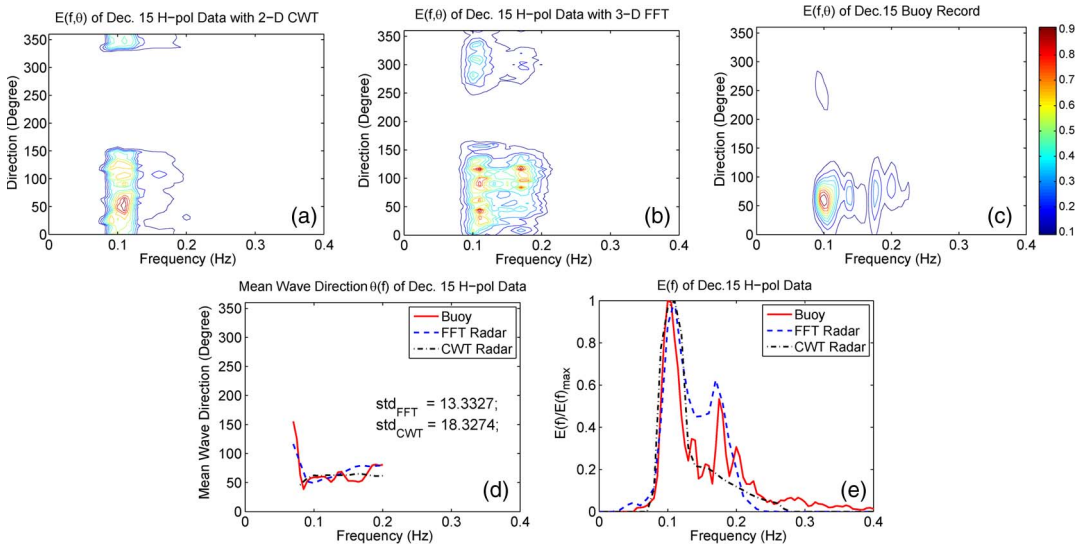

Fig. 4. Comparison of December 15, 2010 results from buoy and H-pol radar data. (a) Two-dimensional CWT-derived directional-frequency spectrum $E_{\mathrm{CWT}}(f,\theta)$. (b) Three-dimensional FFT-derived directional-frequency spectrum $E_{\mathrm{FFT}}(f,\theta)$. (c) Buoy-recorded directional-frequency spectrum $E_{\mathrm{buoy}}(f,\theta)$. (d) Mean wave direction $\theta_p(f)$. (e) Normalized 1-D frequency spectrum $E(f)$.

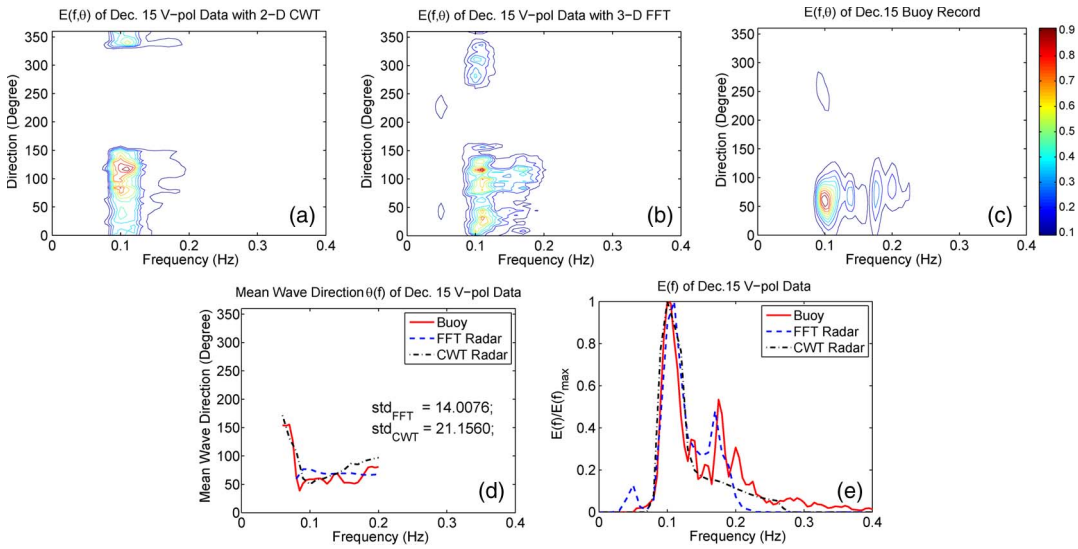

Fig. 5. Comparison of December 15, 2010 results from buoy and V-pol radar data. (a) Two-dimensional CWT-derived directional-frequency spectrum $E_{\mathrm{CWT}}(f,\theta)$. (b) Three-dimensional FFT-derived directional-frequency spectrum $E_{\mathrm{FFT}}(f,\theta)$. (c) Buoy-recorded directional-frequency spectrum $E_{\mathrm{buoy}}(f,\theta)$. (d) Mean wave direction $\theta_p(f)$. (e) Normalized 1-D frequency spectrum $E(f)$.

applied for algorithm validation and analysis. Data from a TRIAXYS wave buoy record collected at the same time were available as the ground truth. Detailed information on the ship-borne radar and buoy is given in Table V. As listed in Table V, the image resolution of the radar field data is $\Delta x = 7.5$ m. Therefore, the corresponding starting β_0 and $\Delta\beta$ values used in this field data test can be calculated as 1.14 and 0.286, respectively, according to (16). The parameters assigned for the wavelet analysis are the same as the land-based dual-polarized data test, as listed in Table III. The parameter used in the MTF process for the Fourier and CWT analysis are given by (22) and (23).

During the field data test, a 20-min radar time series was used for both the 2-D CWT and 3-D FFT analysis, and the results were averaged to acquire the directional-frequency spectrum $\bar{E}(f,\theta)$ in each case. For both methods, wave parameters calculated from these two averages are listed in Table VI, in which the *in situ* wave buoy results collected at the same time are also included. It is obvious that the wave direction $\bar{\theta}$, mean periods T_{01}, and peak frequency f_p retrieved using both methods are close to the buoy record.

Figs. 8 and 9 show the spectra derived from both the 2-D CWT and 3-D FFT algorithms using the ship-borne radar data collected on November 28–29, 2008. The wave buoy information recorded at the same time is also sketched in the figures. The 2-D directional-frequency spectra [see Figs. 8(a)–(c) and 9(a)–(c)] derived by both methods show that the energy distribution is accurately recovered. The mean wave direction spectra $\theta(f)_{\mathrm{FFT}}$ and $\theta(f)_{\mathrm{CWT}}$ [see Figs. 8(d) and 9(d)] retrieved from both methods agree well with those from the buoy

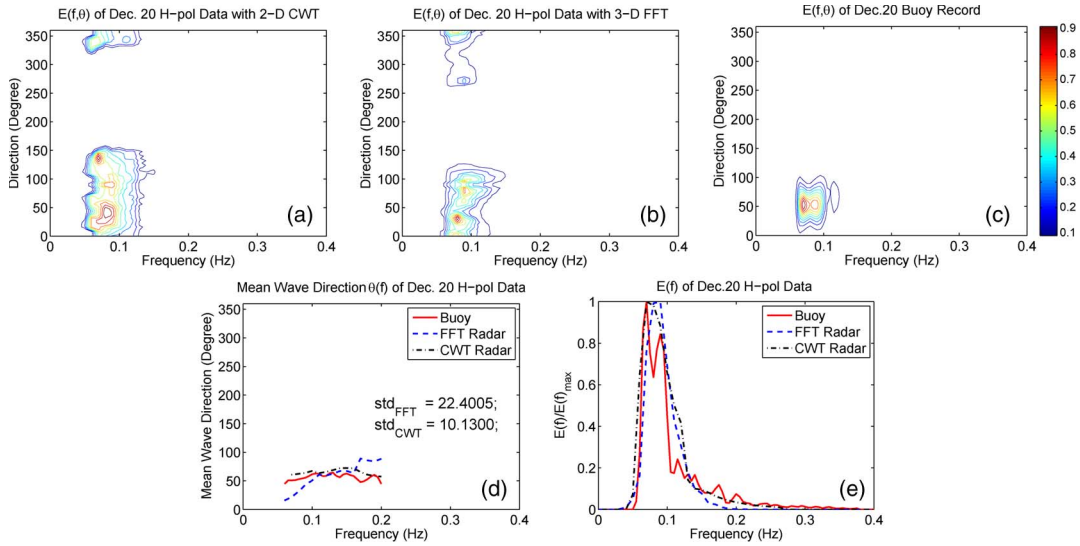

Fig. 6. Comparison of December 20, 2010 results from buoy and H-pol radar data. (a) Two-dimensional CWT-derived directional-frequency spectrum $E_{\mathrm{CWT}}(f,\theta)$. (b) Three-dimensional FFT-derived directional-frequency spectrum $E_{\mathrm{FFT}}(f,\theta)$. (c) Buoy-recorded directional-frequency spectrum $E_{\mathrm{buoy}}(f,\theta)$. (d) Mean wave direction $\theta_p(f)$. (e) Normalized 1-D frequency spectrum $E(f)$.

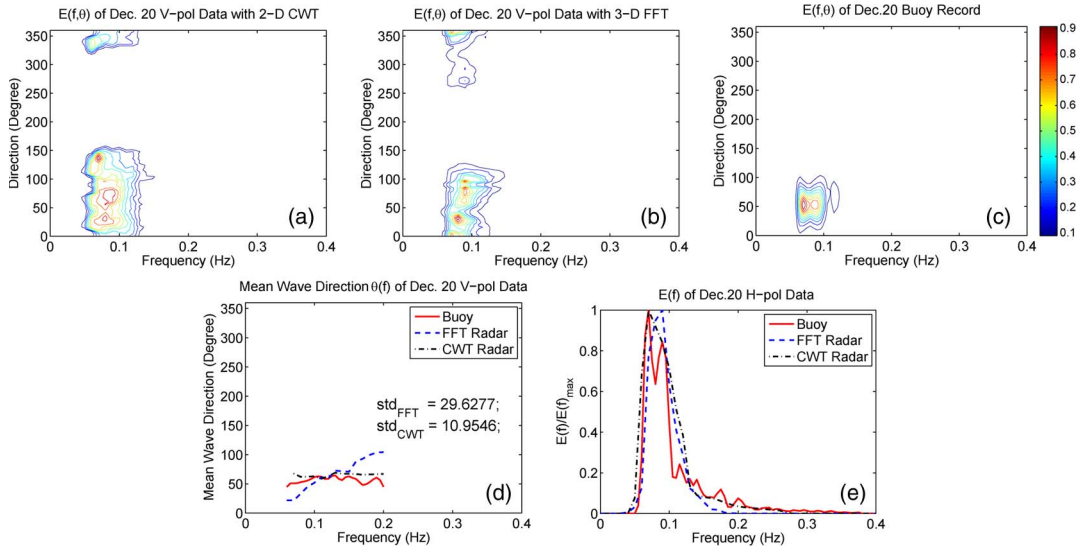

Fig. 7. Comparison of December 20, 2010 results from buoy and V-pol radar data. (a) Two-dimensional CWT-derived directional-frequency spectrum $E_{\mathrm{CWT}}(f,\theta)$. (b) Three-dimensional FFT-derived directional-frequency spectrum $E_{\mathrm{FFT}}(f,\theta)$. (c) Buoy-recorded directional-frequency spectrum $E_{\mathrm{buoy}}(f,\theta)$. (d) Mean wave direction $\theta_p(f)$. (e) Normalized 1-D frequency spectrum $E(f)$.

TABLE V
SHIP-BORNE RADAR AND BUOY DATA INFORMATION

Radar System Specification	
Collecting date	11/28/2008; 11/29/2008
Starting time	15:00:00 (GMT); 07:00:00 (GMT)
Radar location	42.3082N,61.9409W; 42.3913N,61.8723W
Antenna angular speed	28 r.p.m.
The radar range resolution	7.5 m/pixel
Generated Image Size	575×575 pixels
Buoy Information	
Collecting date	11/28/2008; 11/29/2008
Starting time	15:00:00 (GMT); 07:00:00 (GMT)
Buoy location	42.3133N,61.9366W; 42.3602N,61.8598W
Significant wave height	2.58 m; 2.14 m

TABLE VI
COMPARISON OF DERIVED PARAMETERS FROM SHIP-BORNE RADAR DATA AND BUOY RECORDS

Wave parameters	θ (°)	T_{01} (s)	f_p (Hz)	H_s (m)
Date	Nov. 28, 2008			
3-D FFT	105.41	10.43	0.092	2.62
2-D CWT	103.41	9.95	0.095	2.21
Buoy Record	109.39	9.96	0.093	2.58
Date	Nov. 29, 2008			
3-D FFT	103.14	11.27	0.082	1.97
2-D CWT	108.64	10.02	0.083	1.92
Buoy Record	107.70	9.67	0.083	2.14

record. In Fig. 9(d), an obvious error is observed in the Fourier-derived mean wave direction curve near 0.15 Hz, whereas the CWT-derived curve recovers the mean wave direction correctly.

Frequency spectra $E(f)$ retrieved by the 2-D CWT analysis in Figs. 8 and 9(e) are also close to the results using the Fourier analysis as well as the buoy record. In Figs. 8(e) and 9(e), very low energy is seen beyond the Nyquist frequency of 0.23 Hz for

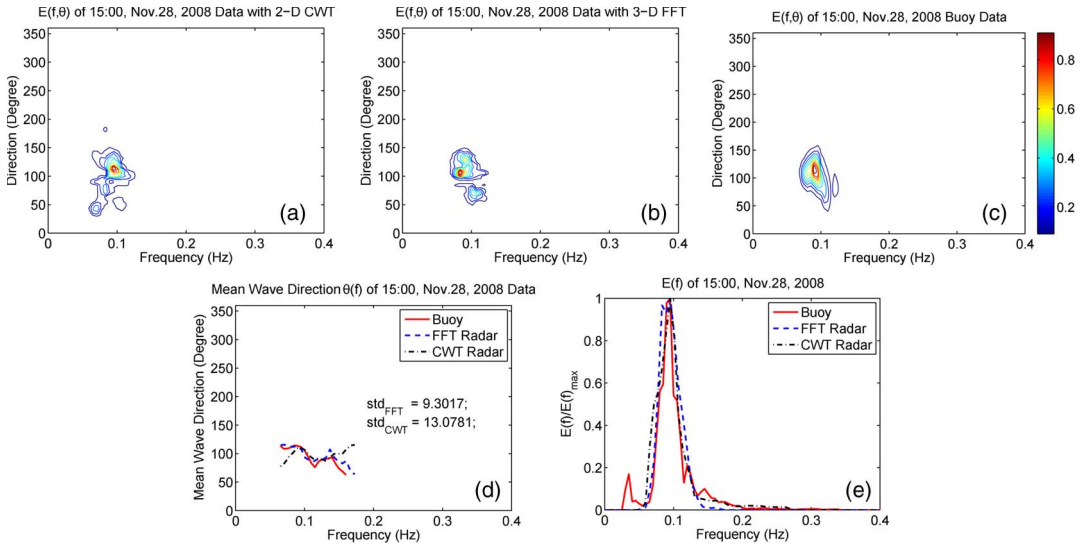

Fig. 8. Comparison of November 28, 2008 results from buoy and ship-borne radar data. (a) Two-dimensional CWT-derived directional-frequency spectrum $E_{\mathrm{CWT}}(f,\theta)$. (b) Three-dimensional FFT-derived directional-frequency spectrum $E_{\mathrm{FFT}}(f,\theta)$. (c) Buoy-recorded directional-frequency spectrum $E_{\mathrm{buoy}}(f,\theta)$. (d) Mean wave direction $\theta_p(f)$. (e) Normalized 1-D frequency spectrum $E(f)$.

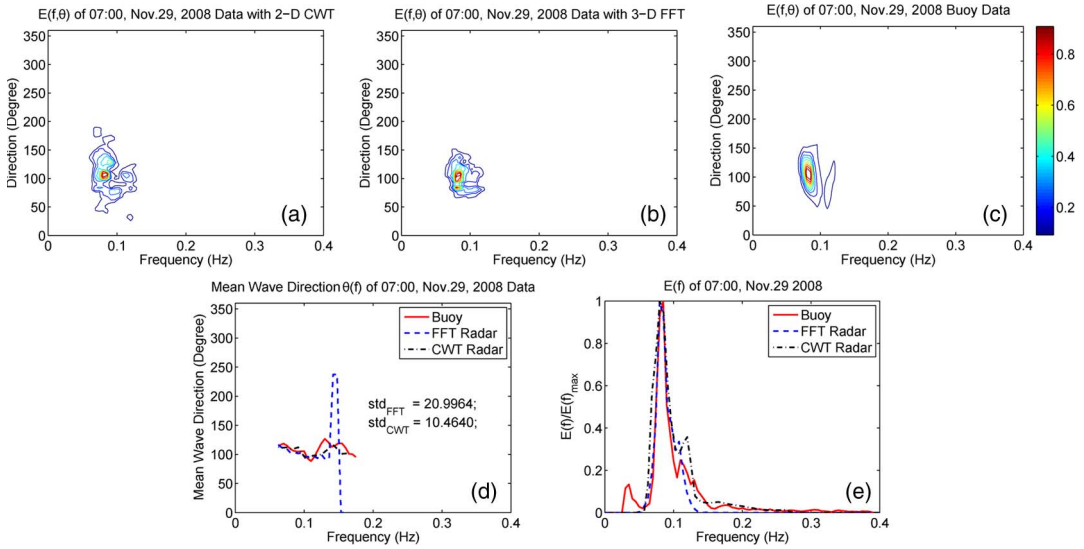

Fig. 9. Comparison of November 29, 2008 results from buoy and ship-borne radar data. (a) Two-dimensional CWT-derived directional-frequency spectrum $E_{\mathrm{CWT}}(f,\theta)$. (b) Three-dimensional FFT-derived directional-frequency spectrum $E_{\mathrm{FFT}}(f,\theta)$. (c) Buoy-recorded directional-frequency spectrum $E_{\mathrm{buoy}}(f,\theta)$. (d) Mean wave direction $\theta_p(f)$. (e) Normalized 1-D frequency spectrum $E(f)$.

the wavelet-based result. This may arise from the superposition of the nonzero tails of the wavelet function.

To verify the robustness of the proposed algorithm, this 21.5-h-long radar data set is used to retrieve the significant wave height, mean period, and wave direction using 3-D FFT and 2-D CWT analysis. The retrieved results are averaged every 30 min for better alignment and comparison with the buoy data (see Fig. 10). It can be seen that both the CWT- and FFT-based radar results agree well with the buoy data except for the period from 23:00 to 00:30, during which the images are almost black (i.e., with very low intensity). Taking the buoy data as ground truth, the root-mean-square errors (RMSE) of the derived significant wave height, mean period, and wave direction are listed in Table VII. Fig. 10(a) provides the current speed of encounter (combination of current and ship). It appears that the current speed does not affect the wave parameter extraction significantly for the data considered here. The results derived from the ship-borne radar data further validate that the proposed 2-D CWT algorithm may be reliably used to extract ocean wave information.

V. Conclusion and Future Work

This paper has provided a new strategy for extracting ocean wave information from nautical radar images based on 2-D CWT analysis. The relation of the wavelet scaling parameters to the minimum distinguishable wavenumber is deduced, and empirical values of the calibration factor β, which refines the optimal $a_{\max}$ under varying wave conditions, are provided. A self-adaptive 2-D CWT wave analysis algorithm is designed

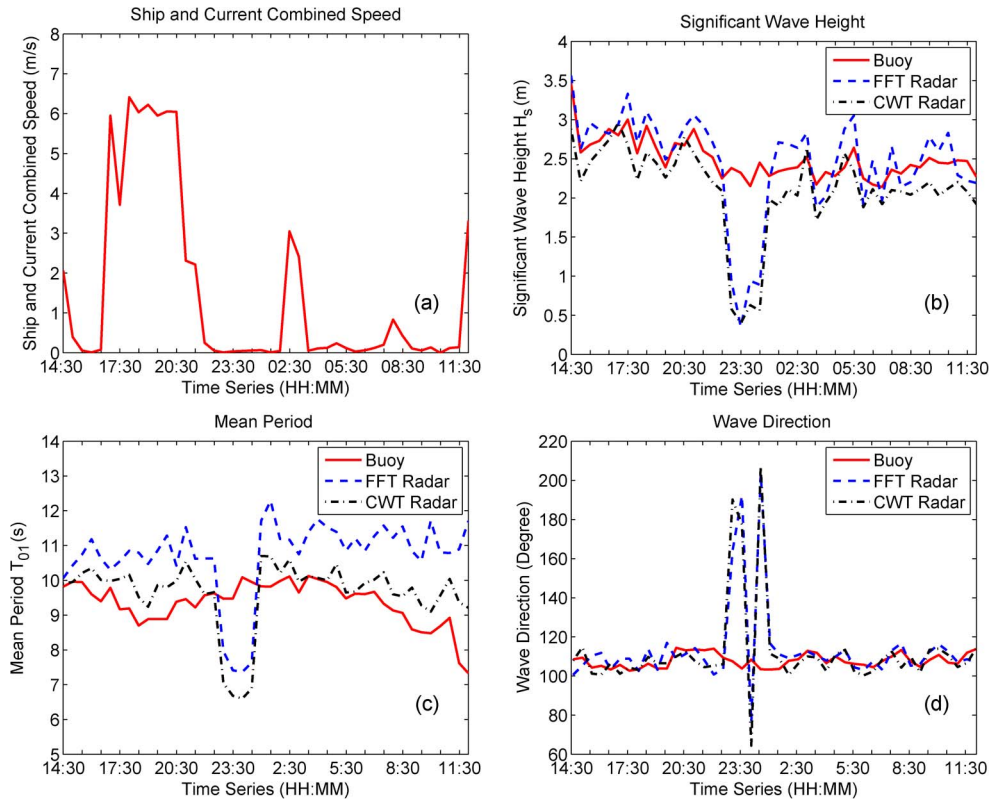

Fig. 10. Results derived from the ship-borne radar data collected on November 28–29, 2008. (a) Combined speed of current and ship. (b) Comparison of significant wave height H_s. (c) Comparison of mean period T_{01}. (d) Comparison of wave direction θ.

TABLE VII
RMSEs OF FFT- AND CWT-BASED WAVE PARAMETERS FROM THE SHIP-BORNE RADAR DATA

Method	3-D FFT			2-D CWT		
Parameters	H_s (m)	$T_{01}(s)$	θ (°)	H_s (m)	T_{01} (s)	θ (°)
RMSE	0.53	1.91	22.96	0.61	1.15	24.18

using an iterative verification process involving the tabulated calibration factors β for different T_{01} values. Both land-based dual-polarized radar field data and ship-borne radar field data are used for algorithm verification. For the experimental data analyzed here, wave spectra parameters using the proposed method are close to the buoy reference and to those derived from the conventional 3-D FFT method. Moreover, it appears that reliable ocean wave information can be extracted from both the H-pol and V-pol data using modified MTFs.

In this research, the 3-D FFT method requires less than 2 s to process one sequence of 32 radar images, whereas the proposed 2-D CWT method usually requires 300–1000 s to process the same quantity of data. However, in our CWT-based analysis, only eight images are required to obtain one result. The computation cost of the CWT algorithm also depends on the choice of initial β_0 and β. Small initial β_0 and β will take more time to obtain a satisfactory result. It should be noted that the FFT analysis used the MATLAB built-in functions, whereas the CWT routines were programmed using MATLAB; however, to date, no attempt has been made to optimize the latter. The purpose of the work presented here has been to provide a proof of concept for the application of the CWT in wave parameter estimation. Having obtained significant success in this regard, the next step will involve optimization of the code to reduce the computational cost. The effect of current velocity on the performance of the algorithm is not considered. Moreover, directional ambiguity inherently exists in the wavenumber spectrum obtained from the 2-D CWT analysis. Here, the ambiguity is removed by referencing the buoy data. The work to date suggests that a 3-D wavelet analysis for the estimation of currents and the possible elimination of the wave directional ambiguity should be explored [17].

ACKNOWLEDGMENT

The authors would like to thank Rutter Technologies and Defence Research and Development Canada for providing the radar field data and Dr. L.-C. Wu for the constructive discussions on this research.

REFERENCES

[1] F. F. Wright, "Wave observation by shipboard radar," *Ocean Sci. Ocean Eng.*, vol. 1, pp. 506–514, 1965.
[2] I. R. Young, W. Rosenthal, and F. Ziemer, "A three-dimensional analysis of marine radar images for the determination of ocean wave directionality and surface currents," *J. Geophys. Res.*, vol. 90, no. C1, pp. 1049–1059, Jan. 1985.
[3] J. C. Nieto Borge, R. G. Rodriguez, K. Hessner, and I. P. Gonzales, "Inversion of marine radar images for surface wave analysis," *J. Atmos. Ocean. Technol.*, vol. 21, no. 8, pp. 1291–1300, Aug. 2004.
[4] P. Izquierdo, C. Guedes-Soares, J. C. Nieto-Borge, and G. R. Rodriguez, "A comparison of sea-state parameters from nautical radar images and buoy data," *Ocean Eng.*, vol. 31, no. 17/18, pp. 2209–2225, Dec. 2004.

[5] C. M. Senet, J. Seemann, and F. Ziemer, "The near-surface current velocity determined from image sequences of the sea surface," *IEEE Trans. Geosci. Remote Sens.*, vol. 39, no. 3, pp. 492–505, Mar. 2001.
[6] W. Huang, E. W. Gill, and J. An, "Iterative least-squares-based wave measurement using X-band nautical radar," *IET Radar Sonar Navig.*, to be published.
[7] J. C. Nieto-Borge, K. Hessner, P. Jarabo-Amores, and D. de la Mata-Moya, "Signal-to-noise ratio analysis to estimate ocean wave heights from X-band marine radar image time series," *IET Radar Sonar Navig.*, vol. 2, no. 1, pp. 35–41, Feb. 2008.
[8] R. Gangeskar, "An algorithm for estimation of wave height from shadowing in X-band radar sea surface images," *IEEE Trans. Geosci. Remote Sens.*, vol. 52, no. 6, pp. 3373–3381, Jun. 2014.
[9] Z. Chen, Y. He, B. Zhang, Z. Qiu, and B. Yin, "A new algorithm to retrieve wave parameters from marine X-band radar image sequences," *IEEE Trans. Geosci. Remote Sens.*, vol. 52, no. 7, pp. 4083–4091, Jul. 2014.
[10] G. E. Carlson, "Wavelet processing of SAR ocean wave images," in *Proc. IEEE IGARSS*, Firenze, Italy, Jul. 1995, vol. 1, pp. 679–681.
[11] M. C. Huang, "Wave parameters and functions in wavelet analysis," *Ocean Eng.*, vol. 31, no. 1, pp. 111–125, Jan. 2004.
[12] S. R. Massel, "Wavelet analysis for processing of ocean surface wave records," *Ocean Eng.*, vol. 28, no. 8, pp. 957–987, Aug. 2001.
[13] L. C. Wu, L. Z. H. Chuang, D. J. Doong, and C. C. Kao, "Ocean remotely sensed image analysis using two-dimensional continuous wavelet transform," *Int. J. Remote Sens.*, vol. 32, no. 23, pp. 8779–8798, Dec. 2011.
[14] L. C. Wu, L. Z. H. Chuang, D. J. Doong, and C. C. Kao, "Quantification of non-homogeneity from ocean remote-sensing images using two-dimensional continuous wavelet transforms," *Int. J. Remote Sens.*, vol. 32, no. 5, pp. 1303–1318, Mar. 2011.
[15] L. Z. H. Chuang, L. C. Wu, D. J. Doong, and C. C. Kao, "Two-dimensional continuous wavelet transform of simulated spatial images of waves on a slowly varying topography," *Ocean Eng.*, vol. 35, no. 10, pp. 1039–1051, Jul. 2008.
[16] D. J. Doong, L. C. Wu, and C. C. Kao, "Spatial wave fields extracted from marine radar images by wavelet transform," in *Proc. 3rd Chinese-German Joint Symp. Coastal Ocean Eng.*, Tainan, Taiwan, Nov. 2006, pp. 1–13.
[17] D. J. Doong, L. C. Wu, C. C. Kao, and L. Z. H. Chuang, "Wavelet spectrum extracted from coastal marine radar images," in *Proc. ISOPE*, Honolulu, HI, USA, May 2003, pp. 258–264.
[18] X. B. Feng, Y. X. Yan, and W. Zhang, "Application of two-dimensional wavelet transform in near-shore X-band radar images," *J. Hydrodynamics*, vol. 23, no. 2, pp. 179–186, Apr. 2011.
[19] J. An, W. Huang, and E. Gill, "2-D continuous wavelet based algorithm for extracting wave information from nautical radar images," in *Proc. IEEE RadarCon*, Ottawa, ON, Canada, May 2013, pp. 1–6.
[20] J. P. Antoine, R. Murenzi, P. Vandergheynst, and S. T. Ali, *Two Dimensional Wavelets and Their Relatives*. Cambridge, U.K.: Cambridge Univ. Press, 2004.
[21] D. Jordan, R. W. Miksad, and E. J. Powers, "Implementation of the continuous wavelet transform for digital time series analysis," *Rev. Sci. Instrum.*, vol. 68, no. 3, pp. 1484–1494, Mar. 1997.
[22] J. An, W. Huang, and E. Gill, "An enhanced algorithm for wave information extraction from X-band nautical radar images," in *Proc. OCEANS*, Hampton Roads, VA, USA, Oct. 2012, pp. 1–5.
[23] W. Huang and E. Gill, "Surface current measurement under low sea state using dual polarized X-band nautical radar," *IEEE J. Sel. Topics Earth Observ. Remote Sens.*, vol. 5, no. 6, pp. 1868–1873, Dec. 2012.
[24] W. Huang and E. Gill, "Simulation analysis of sea surface current extraction from microwave nautical radar images," in *Proc. IEEE ICIP*, Orlando, FL, USA, Oct. 2012, pp. 2673–2676.

Jiaqi An (S'11) was born in Qingdao, China. He received the B.Eng. degree in electronics information engineering from Chongqing University, Chongqing, China, in 2005 and the M.Eng. degree in electrical engineering from Memorial University of Newfoundland (MUN), St. John's, NL, Canada, in 2013.

From 2011 to 2013, he was a Research Assistant and a Teaching Assistant with MUN. His research interests focus on maritime navigation radar signal and image processing algorithm development. He is currently a Computer Engineer with Tata Consultancy Services.

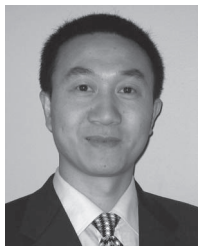

Weimin Huang (M'10–SM'13) received the B.S., M.S., and Ph.D. degrees in radio physics from Wuhan University, Wuhan, China, in 1995, 1997, and 2001, respectively. He completed the M.Eng. degree and a Postdoctoral Fellowship in engineering electromagnetics at Memorial University of Newfoundland (MUN), St. John's, NL, Canada.

He recently joined the Faculty of Engineering and Applied Science, MUN, as an Assistant Professor after working as a Design Engineer at Rutter Technologies. His past and present research involves the mapping of oceanic surface parameters via high-frequency ground wave radar and, more recently, target detection and tracking in ocean clutter using marine radar.

Eric W. Gill (M'00–SM'05) received the B.Sc. degree in physics and the M.Eng. and Ph.D. degrees in electrical engineering from Memorial University of Newfoundland (MUN), St. John's, NL, Canada, in 1977, 1990, and 1999, respectively.

In 1977, he was a Lecturer in physics with the College of the North Atlantic (formerly, Cabot Institute of Applied Arts and Technology). Since 2000, he has been with the Faculty of Engineering and Applied Science, MUN, where he is currently a Professor carrying out teaching and research in theoretical and applied electromagnetics. His special interest lies in the scattering of high-frequency electromagnetic radiation from time-varying randomly rough surfaces, with particular application to the use of ground wave radar in remote sensing of the marine environment.

Dr. Gill is a member of the American Geophysical Union.